Computational modeling of the structure relaxation and dispersion thermodynamics of pristine and modified cellulose nanocrystals in solution

Stanislav R. Stoyanov, Olga Lyubimova, Sergey Gusarov, and Andriy Kovalenko

KEYWORDS: Statistical-mechanical 3D-RISM-KH molecular theory of solvation, Functionalized cellulose nanocrystals, Hydrogen bonding, Solvation free energy, Solvation thermodynamics, Effective interaction, Aqueous electrolyte solution, Non-polar solvent, Ionic liquid

SUMMARY: Cellulose nanocrystals (CNC) exhibit superior mechanical properties and attracted attention as reinforcing additives in polymer nanocomposites. Largescale use of CNC in polymer and biocomoposite materials is currently limited due to its low solubility in nonpolar solvents. We employ a multiscale modeling platform based on the 3D-RISM-KH molecular theory of solvation to study the solvation structure and effective interactions of pristine, sulfonated, and esterified CNC in water, aqueous NaCl solution, an ionic liquid, and benzene. Insights from these studies are intended to help rationally design grafted CNC particles with improved dispersion and preserved mechanical properties that can be more effectively incorporated into materials as reinforcement additives.

ADDRESSES OF THE AUTHORS: S. R. Stoyanov^{1,2,3}, O. Lyubimova^{1,4}, S. Gusarov¹, A. Kovalenko^{1,4,*}

¹National Institute for Nanotechnology, National Research Council of Canada, 11421 Saskatchewan Dr., Edmonton, Alberta, T6G 2M9, Canada, ²Department of Chemical and Materials Engineering, University of Alberta, Edmonton, Alberta, T6G 2V4, Canada, ³Canmet Energy Technology Centre, Natural Resources Canada, Devon, Alberta, T9G 1A8, Canada, ⁴Department of Mechanical Engineering, University of Alberta, Edmonton, Alberta, T6G 2G8, Canada

*Corresponding author e-mail:

Andriy.Kovalenko@nrc-cnrc.gc.ca

Cellulose nanocrystals (CNC), the smallest building blocks of cellulose that carry its physical properties, are a biocompatible and biodegradable material with mechanical properties comparable to reinforcement materials, such as carbon fibers, carbon nanotubes, and steel (Lahiji et al. 2010; Hamad 2006). The CNC can be produced in a sustainable and viable bulk process, unlike other nanomaterials (e.g., carbon nanotubes) that are typically produced in small amounts and at a very high cost (Postek et al. 2008). The outstanding mechanical properties of CNC (Lahiji et al. 2010) make it very attractive as reinforcing additive in nanocomposite materials (Siqueira et al. 2010; Zainuddin et al. 2013; de Mesquita et al. 2012; Khan et al. 2013; Chen et al. 2012), hydrogels (Abitbol et al. 2011; Dorris, Gray 2012; Kelly et al. 2013, Lin, Dufresne 2013; Yang et al. 2013) and foams (Wik et al. 2011; Holt et al. 2010),

as well as specialized security inks (Zhang et al. 2012; Picard et al. 2012). Suspensions of cellulose nanocrystals display a phase separation into clear isotropic and structured chiral nematic phases above concentration (Dong et al. 1996) and upon drying from iridescent chiral nematic films (Beck et al. 2011; Shopsowitz et al. 2012; Kelly et al. 2012). Large-scale applications of CNC in nanocomposites require modifications to tune up its surface properties thus enhancing its solubility in nonpolar solvents and compatibility with polymer matrices (Hasani et al. 2008). The CNC have been extensively manipulated to provide a rich suite of new materials and platforms for further transformations (Habibi et al. 2010). Several methods for CNC surface modification have been developed, including grafting (Araki et al. 2007; Montanari et al. 2005; Wang et al. 2007), self-assembly (Cranston, Gray 2006), and surfactants (Gousse et al. 2002). Effective surface modifications must provide sufficient solubility tune up without altering the CNC interintramolecular hydrogen bonding network deteriorating crystallinity and mechanical properties.

Molecular dynamics (MD) simulation studies have shown that finite model crystals of both I_{α} (Yui, Hayashi 2008) and I_{β} cellulose (Matthews et al. 2006; Matthews et al. 2011; Paavilainen et al. 2011) develop a right-hand twist as a result of solvation in water. The hydrogen bonding network of cellulose is also investigated by using quantum mechanics — molecular dynamics (QM-MD) methods (Qian 2008). The solvation dynamics of cellulose oligomers is also explored using replica exchange MD (Shen, Gnanarakan et al. 2009). Recently, Hirata and coworkers have reported MD simulations of protein docking on cellulose I_{α} surfaces, followed by a 3D-RISM-KH evaluation of the solvation free energy and binding energy effects for the docked configuration (Yui et al. 2010).

Solvation thermodynamics modeling is crucial for understanding dispersion, self-assembly and adsorption of macromolecules on surfaces in the presence of solvents. The statistical-mechanical molecular theory of solvation, also known as three-dimensional reference interaction site model with the Kovalenko-Hirata closure approximation (3D-RISM-KH) (Kovalenko, Hirata 1999; 2000; Kovalenko 2003; Kovalenko 2013) is a powerful methodology capable of predicting solvation processes in chemical and biomolecular nanosystems. Multiscale modeling employing the 3D-RISM-KH theory provides detailed and accurate atomic-scale insights that can accelerate development of advanced materials based on CNC (Stoyanov et al. 2013; Lyubimova et al. 2014). The 3D-RISM-KH molecular theory of solvation properly accounts in a single formalism for both electrostatic and non-polar forces, including hydrophobic and hydrogen

bonding effects, in chemical systems with various solvents (Kovalenko 2003; Gusarov et al. 2006; Casanova et al. 2007; Kovalenko 2013) and ionic liquids (Malvaldi et al. 2009), and reproduces structural and phase transitions in simple and complex liquids and solutions in a wide range of thermodynamic conditions (Kovalenko, Hirata 2001a; 2002; Yoshida et al. 2002) and in nanoporous confinement (Kovalenko, Hirata 2002). The 3D-RISM molecular theory of solvation has been applied to a wide range of problems, including self-assembly, conformational transitions, and function related properties of synthetic organic supra-molecular rosette nanotube nanosystems (Moralez et al. 2005; Johnson et al. 2007; Chhabra et al. 2010; Yamazaki et al. 2010) and biomolecular architectures (Yamazaki et al. 2008; Yamazaki, Kovalenko 2009, Li et al. 2009; Genheden et al. 2010; Yoshida et al. 2009; Blinov et al. 2010; Blinov et al. 2011; Stumpe et al. 2001) as well as gelation activity (Lyubimova et al. 2011; Liu et al. 2011; Kovalenko et al. 2012), network-forming fluids in porous media (Kovalenko, Hirata 2001a, 2001b; Kovalenko, 2004; Tanimura et al. 2007), liquid flow at structured surfaces (Kobryn, Kovalenko 2008), for prediction of asphaltene aggregation (Stoyanov et al. 2008; Costa et al. 2012), and adsorption on mineral surfaces (Stoyanov et al. 2011; Fafard et al. 2013). Recently, we employed the 3D-RISM-KH method to gain insights into the effect of hemicellulose composition of the nanoscale forces acting on plant cell walls and contributing to biomass recalcitrance (Silveira et al. 2013). Based on the first principles of statistical mechanics, the 3D-RISM-KH theory is a unique method that enables proper account of chemical specificities in the solvation structure and thermo-dynamics of very large and complex nanosystems (Kovalenko 2013) by far not feasible with other methods like molecular simulations and/or continuum solvation models.

Multiscale modeling of the relaxation and dispersion of larger CNC particles with surface charge for rational design of commercially available sulfonated CNC in aqueous electrolyte solutions has been performed (Lyubimova et al. 2014). The driving forces of CNC relaxation in solution, electric double layer, nanocolloidal behavior, and chiral nematic ordering, as well as the effect of surface chemical modifications on dispersion thermodynamics in industrially-relevant solvents are also investigated (Stoyanov et al. 2013; Lyubimova et al. 2014).

Here, we employ the 3D-RISM-KH molecular theory of solvation to predict the effective forces that control the dispersion of pristine and modified I_α and I_β CNC particles in a variety of solvents. Both the I_α and I_β phases of cellulose are addressed as these occur naturally and can interconvert. The results indicate that the surface properties of CNC can be tuned to control its dispersion in non-polar solvents used in industrial polymerization processes and ionic liquids used in chemical synthesis. Moreover, we present insights into the CNC-water hydrogen bonding rearrangements and right-hand twist that occur upon relaxation, based on molecular dynamics simulations in aqueous solution.

Computational Methods

3D-RISM-KH theory overview

The theory employs the 3D-RISM integral equation

$$h_{\gamma}(\mathbf{r}) = \sum_{\alpha} \int d\mathbf{r}' c_{\alpha}(\mathbf{r} - \mathbf{r}') \chi_{\alpha\gamma}(r')$$
 [1]

complemented with the Kovalenko-Hirata (KH) closure approximation

$$g_{\gamma}(\mathbf{r}) = \begin{cases} \exp(d_{\gamma}(\mathbf{r})) & \text{for } d_{\gamma}(\mathbf{r}) \le 0 \\ 1 + d_{\gamma}(\mathbf{r}) & \text{for } d_{\gamma}(\mathbf{r}) > 0 \end{cases}$$
 [2]

$$d_{\gamma}(\mathbf{r}) = -u_{\gamma}(\mathbf{r})/(k_{\rm B}T) + h_{\gamma}(\mathbf{r}) - c_{\gamma}(\mathbf{r}),$$

where $h_{\nu}(\mathbf{r})$ is the 3D total correlation function of solvent site γ related to the 3D site density distribution function by $g_{\nu}(\mathbf{r}) = h_{\nu}(\mathbf{r}) + 1$; $c_{\nu}(\mathbf{r})$ is the 3D site direct correlation function which has the asymptotics of the solute-solvent site interaction potential, $c_x(\mathbf{r}) \sim -u_x(\mathbf{r})/(k_B T)$; the site-site susceptibility of pure solvent $\chi_{\alpha\gamma}(r)$ is an input to the 3D-RISM calculation, and indices α and γ enumerate all sites on all sorts of solvent species; $u_{\nu}(\mathbf{r})$ is the 3D interaction potential between the whole solute and solvent site γ specified by a molecular force field, and k_BT is the Boltzmann constant times the solution temperature. The KH closure (2) nontrivially combines the so-called mean spherical approximation (MSA) and hypernetted chain (HNC) approximation, the former being automatically applied to the spatial regions of solvent density enrichment $(g_{x}(\mathbf{r})>1)$ such as association peaks, and the latter to those of solvent density depletion $(g_{\lambda}(\mathbf{r})<1)$, including the repulsive core.

The site-site susceptibility of solvent $\chi_{\alpha\gamma}(r)$ breaks up into the intra- and intermolecular terms,

$$\chi_{\alpha\gamma}(r) = \omega_{\alpha\gamma}(r) + \rho_{\alpha}h_{\alpha\gamma}(r) , \qquad [3]$$

where the intramolecular correlation function $\omega_{\alpha\gamma}(r)$ for interaction sites α and γ on the same species normalized as $\int d\mathbf{r}\omega_{\alpha\gamma}(r) = 1$ represents the molecular geometry of solvent and for rigid molecules with site separations $l_{\alpha\gamma}$ has the form $\omega_{\alpha\gamma}(r) = \delta(r - l_{\alpha\gamma})/(4\pi l_{\alpha\gamma}^2)$ specified in reciprocal k-space as $\omega_{\alpha\gamma}(r) = j_0(kl_{\alpha\gamma})$, $=j_0(kl_{\alpha\gamma})$ in terms of the zero-order spherical function $j_0(x)$, and $h_{\alpha\gamma}(r)$ is the radial total correlation function between sites α and γ enumerating all sites on all sorts of solvent molecules. In advance to the 3D-RISM-KH calculation, the $h_{\alpha \gamma}(r)$ are obtained from the dielectrically consistent RISM (DRISM) theory (Perkyns, Pettitt 1992a; 1992b) coupled with the KH closure (DRISM-KH theory) (Kovalenko 2003; Kovalenko 2013) which is applied to the bulk solvent (water, organic solvent, electrolyte solution, and ionic liquid in this study).

The solvation free energy $\Delta \mu_u$ ("u" stands for solute particle) is obtained from the 3D-RISM-KH theory in a closed analytical form in terms of a simple integral of the 3D correlation functions:

$$\Delta \mu_{\rm u} = k_{\rm B} T \sum_{\gamma} \rho_{\gamma} \left[d\mathbf{r} \left[\frac{1}{2} h_{\gamma}^{2}(\mathbf{r}) \Theta(-h_{\gamma}(\mathbf{r})) - c_{\gamma}(\mathbf{r}) - \frac{1}{2} h_{\gamma}(\mathbf{r}) c_{\gamma}(\mathbf{r}) \right] \right]$$
[4]

where $\Theta(x)$ is the Heaviside step function.

Under isochoric condition, V=const or ρ_V =const, the solvation free energy is decomposed into the excess

partial molecular entropy and the excess partial solvation

$$\Delta \mu_{\mathbf{u}} = \Delta \varepsilon_{\mathbf{u}} - T \Delta S_{\mathbf{u}, V} \tag{5}$$

by numerically calculating the temperature derivative

$$\Delta S_{u,V} = -\left(\frac{\partial \mu_{u}}{\partial T}\right)_{\rho_{V}} \qquad \Delta \varepsilon_{u} = \Delta \mu_{u} + T\Delta S_{u,V}$$
 [6]

The potential of mean force (PMF) between two CNC nanoparticles at separation d (Fig 1) comprises their Lennard-Jones (LJ) and electrostatic (C) interaction potentials plus the difference between their solvation free energies at separation d and at a large distance d_0 (set in practical calculations as d_0 =20 Å):

PMF
$$(d) = E_{Li}(d) + E_c(d) + \mu(d) - \mu(d_0).$$
 [7]

The solvation structure and free energy are obtained from the first principles of statistical mechanics by solving the 3D-RISM-KH integral equations for the 3D correlation functions, with an input of classical-potential molecular force field. (As distinct from the continuum solvation models, this theory does not involve empirical parameters like solvation cavity size and shape nor empirical non-polar terms fitting (de)solvation and hydrogen bonding effects.) The 3D-RISM-KH theory is presented in detail in Kovalenko 2003; Kovalenko 2013; and the Supporting Information for Silveira et al. 2013.

Computational details

Relaxation of I_{α} CNC particles using MD. Molecular dynamics simulations were performed for $CNC_{q=0;-16}^{l=16}$ particle models. The superscript and subscript denote the number of glucosyl residues l and particle charge q. For neutral particles, the simulations were performed in pure water. For negatively charged sulfated CNC particles, 16 Na⁺ were added to the system for overall neutrality. The initial atomic positions in the unit cell were obtained from the crystallographic unit cell data (Nishiyama et al. 2002). The crystals were created by unit cell translations of $8A \times 6B \times 6C$ for $CNC_{q=0;-16}^{l=16}$. Every time, the CNC particle was placed in the center of the simulation box to provide a separation of about 2 nm of the particle surface from the box walls. The rest of the box was filled with explicit water molecules. Initially, NVT simulations with temperature regulation by Langevin dynamics were performed at T=298.15 K. After relaxation, NPT simulation runs were carried out (Lyubimova et al. 2014).

The CNC particle was modeled with GLYCAM06, a highly consistent and transferable all-atom force field, developed for carbohydrates and glucoconjugates (Kirschner et al. 2008). The extended simple point charge (SPC/E) water model (Berendsen et al. 1987) was employed. Nonbonded parameters for sodium and chloride ions were taken from Koneshan et al. 1998. Molecular dynamics calculations were performed with AMBER11 software (Case et al. 2010). The standard procedure of charge redistribution implemented in AMBER11 was used. The relaxation of the CNC particle in explicit water was run for 6 ns.

Dispersion of unrelaxed I_{α} and I_{β} CNC particles. The DRISM-KH theory was used to obtain the site-site correlation functions of solvents in the following states.

At ambient pressure, water has physical density 0.99705 g/cm³ (number density 0.03334 Å⁻³) and dielectric constant 78.54 at 298 K, and density $0.9718 \text{ g/cm}^3 (0.03251 \text{ Å}^{-3})$ and dielectric constant 60.78 at 353 K. 1.069M aqueous solution of NaCl at 298K has density 1.041 g/cm³, water and ions number density 0.03352 and 6.595·10⁻⁴Å⁻³, respectively, and dielectric constant 78.50. 1.069 M aqueous solution of NaCl at 353K has density 1.016 g/cm³, water and ions number density 0.03271 and 6.435·10⁻⁴ Å⁻³, respectively, and dielectric constant 60.78.

Benzene was chosen as a typical example of non-polar organic solvent. Ambient benzene has physical density 0.87367 g/cm³ and dielectric constant 2.2736 at 298 K (Wohlfarth 1991; Lacmann, Synowietz 1974). We used the all-atom model with the parameters summarized in Kobryn and Kovalenko 2008, as it better reproduces the solvation structure of ambient benzene.

The 1,3-dimethylimidazolium chloride ([mmim]Cl) ionic liquid was selected due to its simple and rigid cation structure. [mmim]Cl at 400K has number density 0.00509 Å^{-3} and dielectric constant 10.0 (Malvaldi et al. 2009). The [mmim]⁺ cation was represented using united atom parameters from Lynden-Bell et al. 2002 and the charges were optimized using the multipole-derived charges procedure at the quadrupole level (Swart et al. 2001), as described in Malvaldi et al. 2009.

The CNC solute was represented with the all-atom polymer-consistent force field (PCFF) of Maple et al. 1988; Sun et al. 1988, as implemented in the Discover software package (Discover 2001). Each atom type was assigned wih PCFF charges and Lennard-Jones potential parameters (Freindorf, Gao 1996) designed to represent hydrogen bonding interactions.

To properly treat electrostatic forces in electrolyte solution with polar molecular solvent and ionic species, the long-range electrostatic asymptotics of all correlation functions is separated out and handled analytically (Kovalenko, Hirata 2000a; 2000b; Kovalenko 2003; Gusarov et al. 2012) in the 3D-RISM-KH Eqs [1]-[2], DRISM-KH equations for the radial site-site correlation functions, Eq [3], and the solvation free energy integral, Eq [4]. The short-range terms are discretized on a grid and the convolution is handled with fast Fourier transform.

For all the solution systems, the DRISM-KH integral equations were discretized on a uniform radial grid of 16384 nodes and size 409.6 Å with resolution 0.025 Å, which ensured high accuracy of solvent correlations. For the finite-length CNC particles in aqueous solution, the 3D-RISM-KH integral equations were discretized on a uniform rectangular 3D grid with resolution 0.5 Å in a 128×128×128 Å cubic supercell. An increase of grid resolution to 0.25 Å for a grid of 256×256×256 nodes in the same supercell size changed the solvation free energy by < 2.0 kcal/mol and the partial molar volume by $< 8.0 \text{ Å}^3$, showing sufficient accuracy. For the periodically-extended CNC particles in water, benzene, and ionic liquid, the 3D-RISM-KH integral equations were solved on a grid of 256×256×128 nodes in a $64\times64\times20.76$ Å supercell.

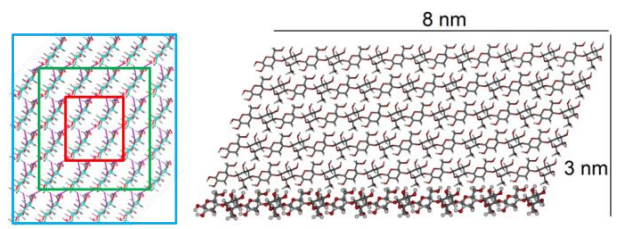


Fig 1 - Cellulose fibril containing 34 glucan chains: Left part: Cross section showing inner (red), intermediate (green) and outer (blue) layers. Right part: Sizes of CNC particle.

The 3D-RISM-KH integral *Eqs* [1]-[2] were converged to a relative root mean square accuracy of 10⁻⁸ and the DRISM-KH equations to an accuracy of 10⁻¹² by using the modified direct inversion in the iterative subspace (MDIIS) accelerated numerical solver (Kovalenko et al.1999; Kovalenko 2003).

Results and Discussion

Relaxation of I_{α} CNC particle

We built a model for the computer simulation of CNC based on the I_{α} crystal structure (Nishiyama et al. 2003) containing 34 chains forming a three-layered cellulose fibril, as shown in *Fig 1*. The inner, intermediate and outer layers shown in blue, green and red rectangles, respectively, undergo structural changes upon relaxation in water. The fibril cross section is approximately 4.3 nm in its longest direction and each chain in the fibril consists of 16 glucose units making 8 nm long particles. This particle cross-section or width is selected as it falls within the experimental range of 4-5 nm for CNC made from soft wood (Habibi et al. 2010).

For this model particle, we have performed structure relaxation using molecular dynamics simulation in a periodic box with dimensions 14.9 nm \times 8.9 nm \times 8.3 nm. The distance between particle surface and the box edges is 2 nm and the space in the box around the particle is filled with water molecules. The aim of this simulation is to relax and equilibrate the model structure in the presence of solvent, mimicking as close as possible the experimental conditions of pristine CNC solvation in aqueous solution. In this neutral particle, the initial charge distribution in the cellulose fibril is inhomogeneous over different faces of the particle (Fig 2a, b). In the crystal, cellulose layers are stacked so that the positively charged groups face the negatively charged groups giving a "crystal-like" charge distribution. We obtain 3D density distributions of solvent species around an unrelaxed CNC particle. It is clearly seen that Cl⁻ anions are concentrated around the particle surface with exposed positively charged groups, while Na⁺ cations are localized on the negatively charged opposite side of the particle ($Fig\ 2c$).

We relax the CNC particle in explicit water solution for 6 ns and analyze the structure after relaxation. We observe a smearing of the charge over the faces (Fig 2d and 2e), which noticeably affects the distribution of the ions around the fibril (Fig 2f). The relaxed particle charge is weakly polarized, as evidenced by the rather even distribution of cations and anions around it. In both unrelaxed and relaxed particles, the ions distributions are calculated using the 3D-RISM-KH theory for a particle in

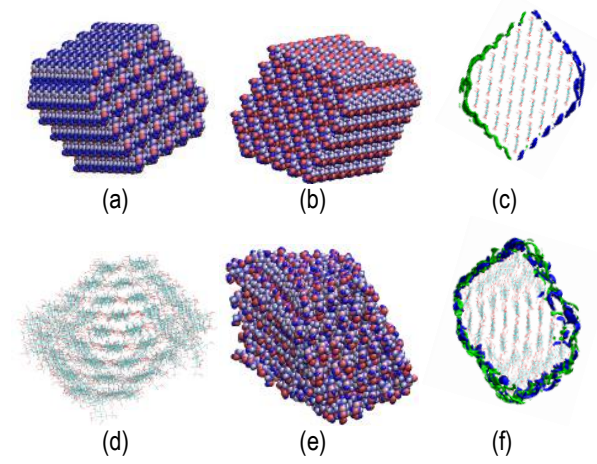


Fig 2 - Pristine CNC particle relaxation in explicit water solution simulated with MD, showing positively (in blue) and negatively (in red) charged atoms. Top: Surface charge distribution of the unrelaxed CNC particle. (a) Faces exposing positively charged groups are predominantly blue colored. (b) Faces exposing negatively charged groups are predominantly red colored. (c) 3D distributions of Na+ (blue) and Cl- (green) around an unrelaxed fibril in aq. NaCl. Bottom: Surface charge distribution of a relaxed CNC particle after 6 ns MD simulation. (d) CNC particle cross section showing right-hand twist. (e) Charge distribution in the relaxed particle. (f) 3D distributions for Na+ (blue) and Cl- (green) around a relaxed fibril in aq. NaCl.

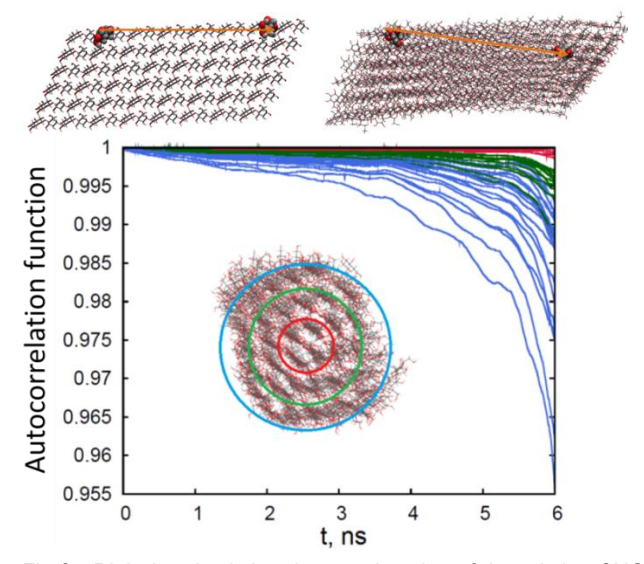


Fig 3 - Right-hand twisting due to relaxation of the pristine CNC particle in explicit water. Top part: Vector between the center of mass of highlighted fragments (third ring from chain ends). Initial unrelaxed and twisted relaxed structures are shown. Bottom part: Time autocorrelation function for vectors shown in top left with colors corresponding to the chain position in the relaxed fibril layer shown in the inset and defined in *Fig 1*, left.

aqueous solution of NaCl at concentration 0.040 mol/kg (Lyubimova et al. 2014).

In addition to a more uniform surface charge distribution upon the relaxation in solution, CNC particles undergo right-hand twisting (Fig 3). To quantify the particle twist and observe its evolution in time we define a vector between the center of mass of the end-fragments of every chain (Fig 3, top left). Upon relaxation, the

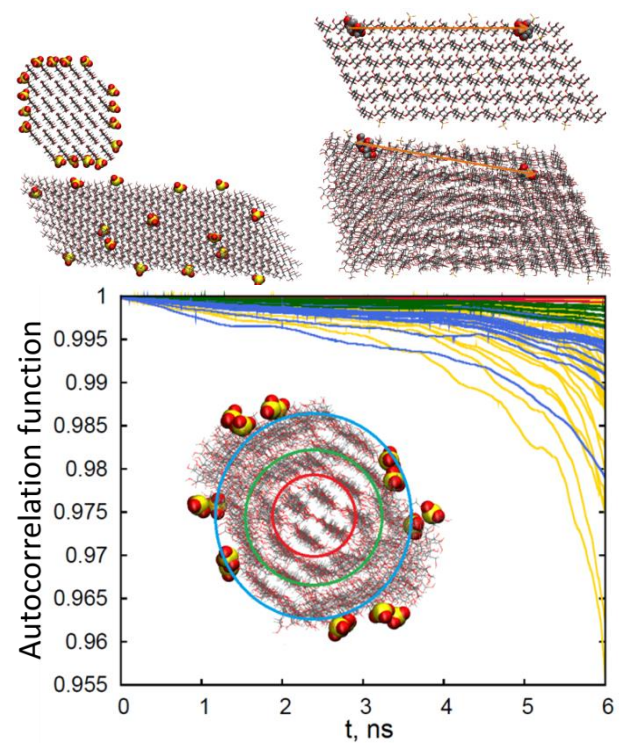
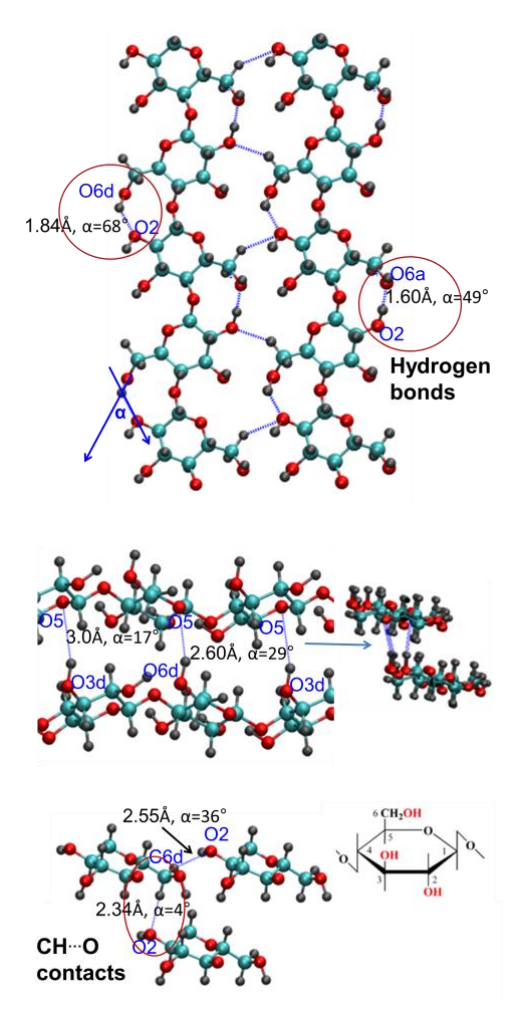


Fig 4 - Relaxation of a sulfonated CNC particle in water. Top left part: Initial unrelaxed particle with 16 SO₃- groups distributed evenly on the particle surface. Particle cross-section and sideview are shown. Top right part: Vectors defined between the center of mass of highlighted fragments (third ring from chain ends) for unrelaxed (top) and relaxed twisted (bottom) structure. Bottom: Time autocorrelation function for vectors defined in top right with colors corresponding to the position of the cellulose chain in the relaxed fibril layers shown in the inset. Yellow curves for the autocorrelation functions of the neutral particle are shown for comparison with Fig 3.

surface cellulose chains undergo substantial twisting (Fig 3, top right). From the vector length and origin over the trajectory, we calculate the time autocorrelation function for every chain and use it to quantify the extent of righthand twisting, as shown in Fig 3, bottom. It should be noted that the degree of twisting of chains is different depending on the chain position in the fibril. The inner layer chains experience minor deviation from the initial crystal structure, as seen in the corresponding time autocorrelation functions (red curves) close to 1.00. The intermediate layer chains (green curves in the time autocorrelation function plot) undergo twisting of 0.995-1.00. The outer layer chains, (blue curves in the time autocorrelation function plot) undergo the largest twisting. The colors in the graph correspond to the CNC particle layers defined in Fig 1 and shown in the time autocorrelation function plot inset after relaxation.

We hypothesize that the initial "crystal-like" highly polarized charge distribution in the CNC particle is one of the driving forces leading to the fibril twisting. There are numerous experiments showing an overall right-hand twist in cellulose microfibrils and microcrystalline cellulose (Hanley et al. 1997; Ellazzouzi-Hafraouzi et al. 2008). Twisting is also reported for MD relaxation of the CNC particle (Paavilainen et al. 2011) with explicit water solvation simulated using the TIP3 water model and



Scheme I - Hydrogen bonding network of I α cellulose showing intra-chain (top) and inter-chain hydrogen bonds (middle) as well as the weaker CH···O contacts (bottom).

OPLS force field extended for carbohydrates (Damm et al. 2001).

The next step taken towards the development of representative CNC models is to build a charged sulfonated particle model. We accomplished this by grafting sulfate groups to some of the cellulose's surface chains. The number of sulfonate groups was taken from elemental analysis (Boluk et al. 2012). We modified 16 glucose units at the C6 position with sulfate groups so as to have 4 substitutions on each face (Fig 4). Each sulfonate group bears one unit of negative charge and the total CNC particle charge is 16e. The estimated surface charge density is $0.3 e/nm^2$, in accordance with the experimental values for sulfonated CNC (Jiang et al. 2010). The MD system setup for the particle relaxation is similar to that of the neutral particle, the only difference being the addition of 16 Na⁺ into the simulation box to achieve overall electrostatic neutrality.

Structure relaxation analysis for the charged particles yields a dependence of the particle twisting similar to that of the neutral particle. In *Fig 4*, a comparison of the largest (outer) layer twist of sulfonated CNC (blue lines) to the largest twist for the neutral particle (yellow lines) indicates that the maximal degree of twisting of charged particle chains is about half of that of the neutral particle,

as evaluated from the time autocorrelation function. It is worth noting that the deviation from the crystal structure upon relaxation is more pronounced in the case of a neutral particle due to the even distribution of the SO₃⁻ grafting sites on all four faces of the particle and reduced face non-equivalency (Lyubimova et al. 2014).

Hydrogen bonding rearrangements of I_{α} CNC particle

The hydrogen bonding network shown in Scheme I is responsible for the stabilization of cellulose microfibrils and pristine CNC (Nishiyama et al. 2002; 2003). The hydrogen bonding interactions shown in the top and middle panels are substantially stronger than the CH^{...}O contacts. The contribution of the latter studied using 3D-RISM-KH has been discussed in Silveira et al. 2013.

In a sulfonated CNC particle placed in water, a new set of hydrogen bonds forms between CNC and water that leads to a rather extensive rearrangement of the cellulose chains accompanied by the right-hand twist described above. In Fig 5, we present the total number of water-CNC hydrogen bonds that occur during a 10 ns MD simulation of a sulfonated $CNC_{q=-16}^{l=16}$ particle as well as the contributions of O atom types and sulfonate groups of CNC. The largest contributions (highlighted with rectangles and arrows) arise from O2 and O6 that in I α cellulose participate in intra-chain hydrogen bonds (Scheme I, top), followed by O3 atoms that participate in inter-chain hydrogen bonds (Scheme I, middle) and those involving the negatively-charged sulfonate groups.

Effective interactions of pristine I_{α} CNC particles

We also study the effective force for removal of a CNC particle (nanofibril) from bulk I_{α} cellulose in aqueous solution at a direction perpendicular to the chains. In Fig 6 (A), we depict a model system of two CNC particles containing 4 parallel cellulose chains of 8 monomers each. We calculate the solvent distribution around these particles as the interparticle distance d is increased. At d =5.6 Å, water and electrolyte can enter between the CNC particles, as shown with the 3D-density distribution function isosurfaces in Fig 6. The isosurfaces for water (A and B) indicate that the go(r) maxima (dark blue) and g_H(r) (light blue) are localized near H and O atoms, respectively, of surface hydroxyl groups of cellulose, indicating that water forms a hydrogen bonding network, as highlighted in the enlarged areas of A and B with arrows and rectangles.

In $Fig\ 6$ (C and D), the 3D density distributions of Na⁺ (purple) and Cl⁻ (green) highlight the charge polarization of the particle faces that helps stabilize cellulose in its crystalline state in bulk. Upon relaxation in solution drive the right-hand twist ($Fig\ 3$ and 4) and to a large extent the hydrogen bonding ($Fig\ 5$) (Stoyanov et al. 2013; Lyubimova et al. 2014).

In Fig 7, we show the PMF between two pristine uncharged and unrelaxed I α particles (Fig 6 (A)). The PMF at separation d Å is defined as the difference between their Lennard-Jones, electrostatic, and solvation free energy terms and those at full separation. The PMF contains the main features of the effective interaction

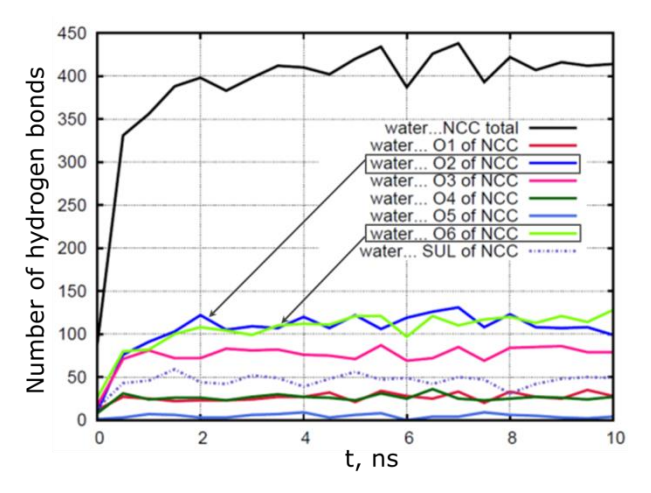


Fig 5 - Water-CNC hydrogen bonding analysis from the relaxation of sulfated I α CNC in water based on a 10 ns MD simulation. The number of water-CNC hydrogen bonds is shown on the y-axis. The largest number of hydrogen bonds, highlighted with rectangles and arrows, are of intra-chain type

among CNC particles in solution. The minima at 2.5 Å and 5.6 Å correspond to stable CNC-CNC hydrogen bonding and CNC solvated with one layer of water, respectively. The absolute minimum at 5.6 Å indicates that cellulose with one hydration shell is more stable than cellulose held together by inter-chain hydrogen bonds, as in the bulk.

The maximum at 4.0 Å corresponds to the energy barrier that has to be overcome upon (dis)aggregation. (Note that this PMF barrier height of about 100-150 kcal/mol is typical for colloids of this size.) From the barriers of disaggregation and solvent expulsion defined in *Fig 7*, we predict the stability of the solvation shell and dispersion preferences of the CNC particles in solution. Aggregation is most favored in water at 353K and least favored in NaCl at 298K. This is related to the dispersion and swelling of cellulose in electrolyte and alkaline solutions (Stoyanov et al. 2013).

Effective interactions of pristine and esterified I_{β} CNC

In order to incorporate CNC in plastics and composites, it is necessary to make it dispersible in the non-polar solvents widely used in the polymers industry. Considering that cellulose contains a large number of surface hydroxyl groups, one way to make it dispersible is to functionalize with aliphatic groups by esterification. We consider pristine and esterified IB cellulose in a hydrophilic solvent (water), a hydrophobic solvent (benzene) and the ionic liquid [mmim]Cl. Ionic liquids are a novel class of non-volatile environmentally-friendly solvents that have attracted the interest of synthetic chemists due to the fundamentally different reaction thermodynamics and kinetics compared to typical molecular solvents (Welton, Wasserschield 2007). The 3D-RISM-KH method predicts the properties of ionic liquids in a remarkable agreement with conclusions drawn from other methods (Malvaldi et al. 2009).

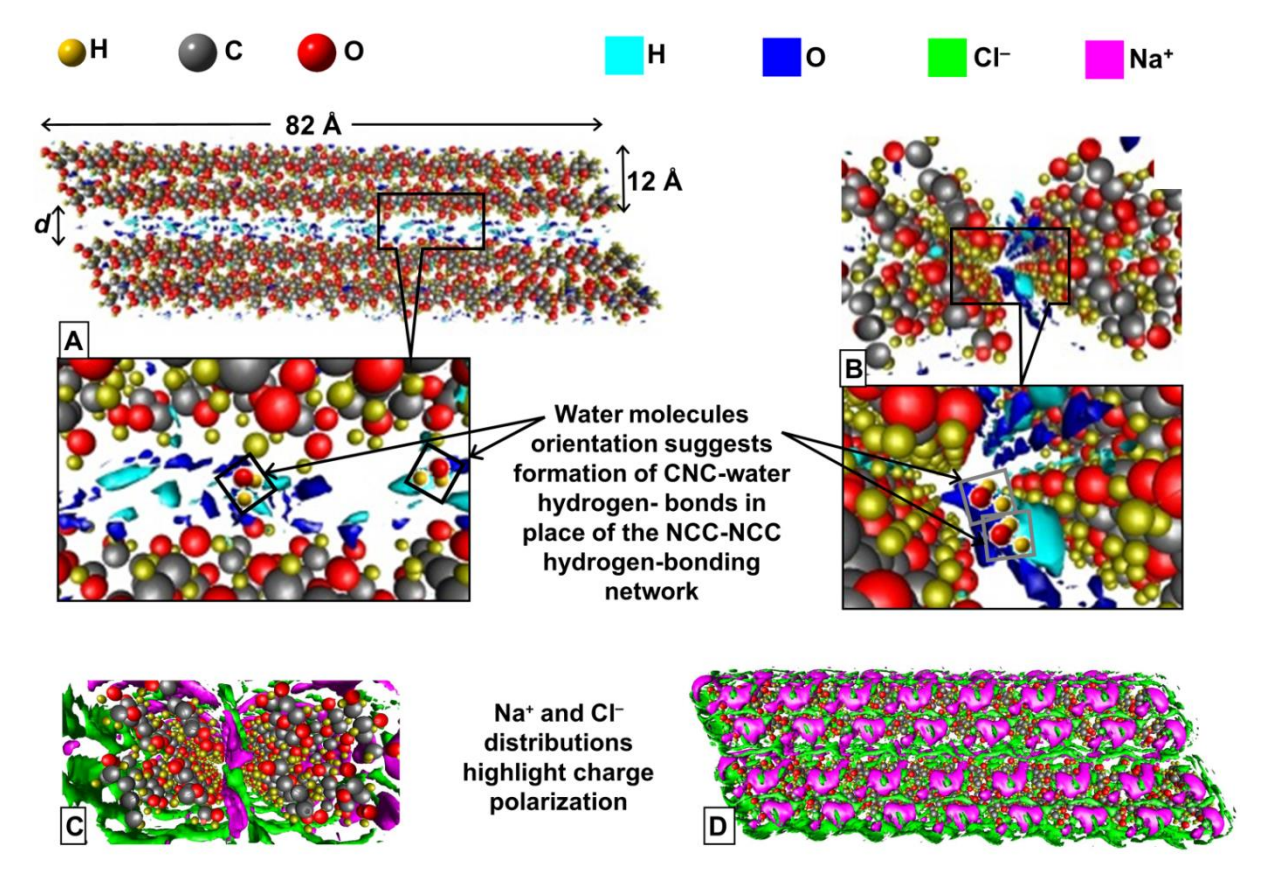


Fig 6 - Water and NaCl distribution around I α CNC aggregate (modeled after Nishiyama et al. 2003) at distance d=5.6 Å, corresponding to the 2nd minimum of the PMF (Fig 7). The 3D distribution function isovalues are g_O = 5.0 and g_H = 2.8 (parts **A** and **B**) as well as g_{Na} = 2.0 and g_C = 2.4 (parts **C** and **D**). Based on the maxima of the 3D distribution functions of O (dark blue) and H (light blue) sites of water, we predict the preferred orientation of water in the space between the disaggregating particles. In the enlarged views highlighted with call boxed in **A** and **B**, we have placed explicit water molecules (in black (**A**) and grey (**B**) boxes) to help visualize the predicted water molecule orientation and the formation of a CNC-water hydrogen bonding network in place of the interparticle hydrogen bonding network that exists in bulk I α cellulose.

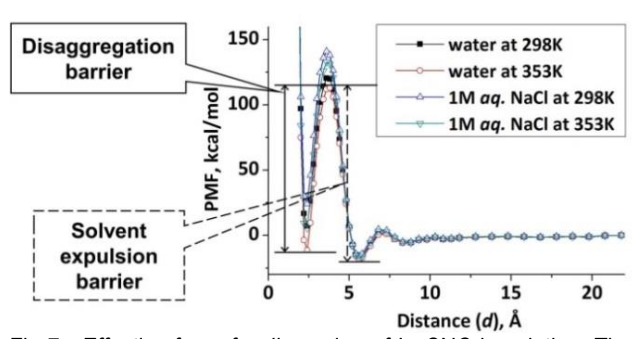


Fig 7 - Effective force for dispersion of I α CNC in solution. The absolute minimum at 5.6 Å indicates that cellulose is more stabilized by a monolayer of water (Fig 6 (**A** and **B**)) than by inter-chain hydrogen bonds.

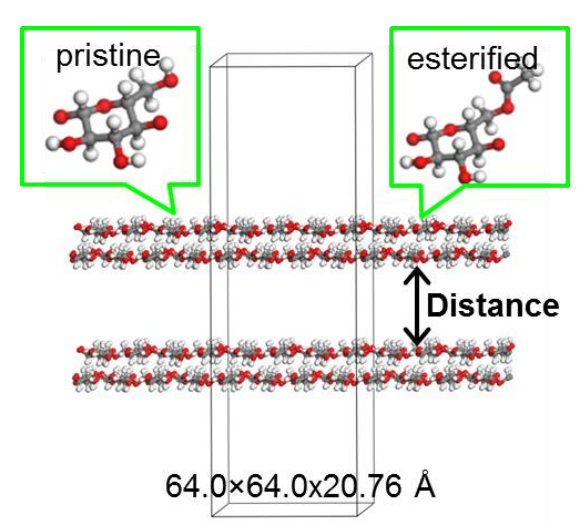


Fig 8 - Pristine and esterified periodically-extended Iβ CNC model. The pristine and esterified monomer structures are shown in the green call boxes. The effective interactions between the two particles in solution are computed as the interparticle distance is varied and the periodic boundary conditions box (shown in grey) is filled with solvent.

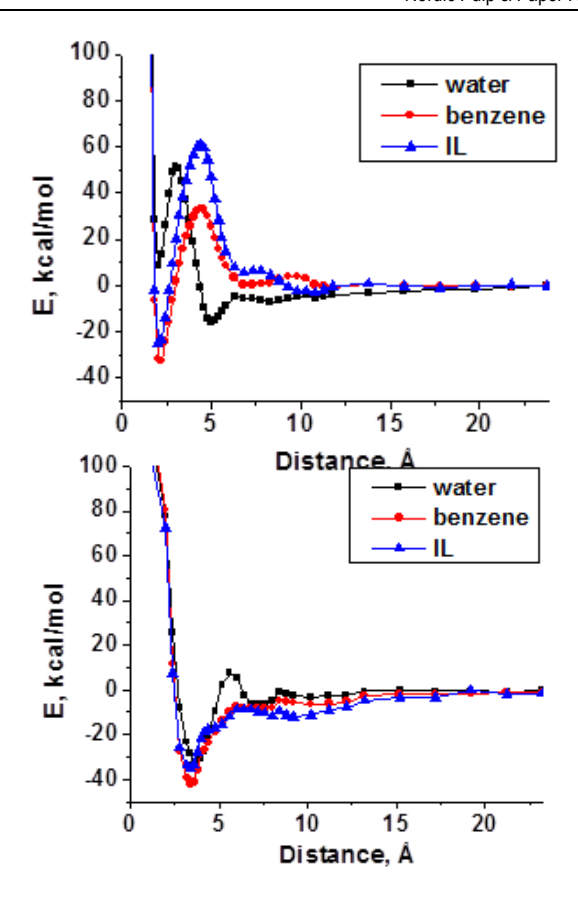


Fig 9 - PMF of pristine (top) and esterified (bottom) periodically-extended I β CNC in the solvents water, benzene and [mmim]Cl ionic liquid (IL) .

In Fig 8, we show a two-particle periodically-extended Iβ CNC rod model that is suitable for prediction of the effective interactions of particles with uniform surface and large aspect ratio. Each particle contains 4 parallel chains of 4 monomers each. Such periodically-extended model is not applicable to Iα cellulose due to its unit cell The pristine Iβ cellulose structure is from type. Nishiyama et al. 2002. In the esterified structure, every primary surface hydroxyl group (O6 atom, Scheme I) is modified to an ethyl ester group and the particle structure is partially relaxed (with constrained cellulose backbone) using molecular mechanics. The monomers of pristine and esterified cellulose are shown in the insets. The effective interactions are computed in water, benzene and ionic liquid as the distance is varied.

In Fig 9, we show the effective force (PMF) plots for pristine and esterified CNC in the top and bottom panels, respectively. The PMF is normalized per periodic unit cell (8 chains, each 4 monomers long, per unit cell in this case). Similar to I α cellulose, the I β cellulose is stabilized in water by a hydration shell, as the absolute minimum is at ~5 Å. The disaggregation barrier for pristine CNC increases in the order water < benzene < [mmim]Cl, indicating that dispersion in water is favorable, whereas in benzene and [mmim]Cl it is not. This behavior is typical for hydrophilic surfaces (Stoyanov et al. 2013).

For esterified CNC, the PMFs in benzene and [mmim]Cl have lower disaggregation barrier than in water, suggesting facilitated dispersion in hydrophobic solvents.

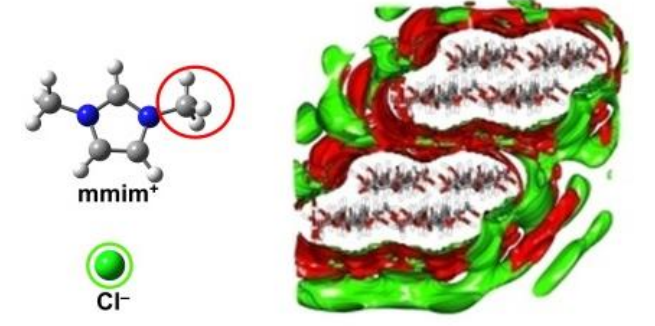


Fig 10 - Solvation structure of the ionic liquid 1,3-dimethylimidazolium chloride [mmim]Cl around a periodically extended pristine I β CNC particle.

The lack of significant solvent expulsion barriers in benzene and ionic liquid suggest weak solvent-solute interaction. This example demonstrates how surface modifications are being employed to tune-up the dispersion properties of CNC in various solvents. For every solute configuration, our platform predicts the solvent orientation based on the solvent distribution function, as presented in *Fig 10* for the ionic liquid [mmim]Cl. In addition to addressing the type of the surface modification, this platform allows prediction of the degree of surface modification necessary to achieve a certain dispersion effect. This is particularly important in industrial processing, where achieving high degrees of surface modification is costly (Stoyanov et al. 2013).

Conclusions

In this work, we present an approach to rational design of CNC surface modifications by employing the multiscale modeling platform that combines quantum chemistry (for derivation of force field parameters, as shown in detail for [mmim]Cl in Malvaldi et al. 2009) with the statisticalmechanical 3D-RISM-KH molecular theory of solvation and with MD simulations. This study addresses the dispersion of cellulose from a crystalline bulk phase in aqueous solution and the stabilization of cellulose nanoparticles by water through hydrogen bonding. Relaxation of the charge polarization of periodic crystalline cellulose (visualized on the Na⁺ and Cl⁻ density distributions) is one of the driving forces of the structural rearrangements upon relaxation of CNC in solution. Another driving force is the increase in the number of hydrogen bonds between glucan chains in the CNC particle. Note that a trigger of this right-hand twist resulting largely from the interchain electrostatics and hydrogen bonding is the inherent chirality of a single glucan polymer chain assuming the flat twofold screw symmetry. Upon sulfuric acid hydrolysis, the grafted surface charges also affect the relaxation. These three factors determine the extent of helical twisting upon relaxation of CNC in aqueous solutions.

Our calculations show that pristine cellulose would not be dispersed in benzene. Upon hydrophobic modification by esterification, dispersion of cellulose becomes favorable. This illustrates the capability of our modeling approach to predict and design surface chemical modifications for CNC compatibilization with organic solvents used in industrial processes.

This theoretical modeling approach presents molecular models of functionalized CNC particles and validates modeling procedures recapitulating the essential properties of CNC, which will be useful for future study of CNC effective interactions and ordered phase formation in electrolyte solutions. In this approach, the nature and concentration of electrolyte solution can be readily varied to perform quick in-silico screening of their effect on the CNC effective interaction strength. The 3D-RISM-KH molecular theory of solvation yields the full solvation thermodynamics by statistical-mechanical sampling of solvent arrangements and orientations around CNC particles. This is by far not feasible using molecular simulations, as it requires sampling of molecular forces in the system tens nanometers large on time up to microand milliseconds long, including solvent and ions around CNC particles as well as in the confined space between them. The latter is most challenging because of the specific binding and slow exchange of both solvent and ions in the CNC solvation shells, particularly in the bound arrangements bridging CNC particles. This problem is inherent in standard MD simulation techniques with free energy calculation by means of thermodynamic integration, free energy perturbation, and umbrella sampling. It also holds in the new simulation techniques extracting free energy from a single MD simulation as an functional of an energy distribution (Matubayashi, Nakahara 2000), which still requires adequate sampling of the slow processes of exchange and specific binding.

In prospective, this multiscale modeling platform can include dissipative particle dynamics (DPD) simulation with coarse-grained force fields obtained from the 3D-RISM-KH theory (Nikolic et al. 2013; Kobryn et al. 2014). Further improvements of the model will include effect of relaxation on the effective interaction between CNC particles in solution.

Acknowledgement

This work was supported by ArboraNano – a Business-led Canadian Forest NanoProducts Network, Alberta Innovates Bio Solutions, NanoAccelerator Program of Alberta Innovates Technology Futures, National Institute for Nanotechnology, and University of Alberta. The authors express their gratitude to Dr. Ron Crotogino and Dr. Nicole Poirier of ArboraNano, Dr. Steve Price and Dr. Ted Szabo of Alberta Innovates Bio Solutions, Dr. Robert Jost of Alberta Innovates Technology Futures, and Dr. Yaman Boluk of the Department of Civil Environmental Engineering, University of Alberta. SRS thanks Dr. John M. A. Villegas for the fruitful discussions. The computations were performed on the high performance computing facilities of WestGrid – Compute/Calcul Canada.

Literature

Abitbol, T., Johnstone, T., Quinn, T.M. and Gray, D.G. (2011) Reinforcement with cellulose nanocrystals of poly(vinyl alcohol) hydrogels prepared by cyclic freezing and thawing. Soft Matter, 7, 2373-2379.

Araki, J., Wada, M. and Kuga, S. (2007) Steric Stabilization of a Cellulose Microcrystal Suspension by Poly(ethylene glycol) Grafting. Langmuir, 17, 21-27.

Beck, S., Bouchard, J. and Berry, R. (2011) Controlling the Reflection Wavelength of Iridescent Solid Films of Nanocrystalline Cellulose. Biomacromolecules, 12, 167-172.

Berendsen, H.J.C., Grigera, J.R. and Straatsma, T.P. (1987) The Missing Term in Effective Pair Potentials. J. Phys. Chem., 91, 6269-6271.

Blinov, N., Dorosh, L., Wishart, D. and Kovalenko, A. (2010) Association thermodynamics and conformational stability of β-sheet Amyloid β (17-42) oligomers: effects of E22Q (Dutch) mutation and charge neutralization. Biophys. J., 98, 282-296.

Blinov, N., Dorosh, L., Wishart, D. and Kovalenko, A. (2011) 3D-RISM-KH approach for biomolecular modeling at nanoscale: thermodynamics of fibril formation and beyond. Molec. Simul., 37, 718-728.

Boluk, Y., Zhao, L. and Incani, V. (2012) Dispersions of Nanocrystalline Cellulose in Aqueous Polymer Solutions: Structure Formation of Colloidal Rods. Langmuir, 28, 6114–6123.

Casanova, D., Gusarov, S., Kovalenko, A. and Ziegler, T. (2007) Evaluation of the SCF combination of KS-DFT and 3D-RISM-KH; Solvation effect on conformational equilibria, tautomerization energies, and activation barriers. J. Chem. Theory. Comput., 3, 458-476.

Case, D.A., Darden, T.A., Cheatham III, T.E., Simmerling, C.L., Wang, J., Duke, R.E., Luo, R., Walker, R.C., Zhang, W., Merz, K.M., Roberts, B., Wang, B., Hayik, S., Roitberg, A., Seabra, G., Kolossváry, I., Wong, K.F., Paesani, F., Vanicek, J., Liu, J., Wu, X., Brozell, S.R., Steinbrecher, T., Gohlke, H., Cai, Q., Ye, X., Wang, J., Hsieh, M.-J., Cui, G., Roe, D.R., Mathews, D.H., Seetin, M.G., Sagui, C., Babin, V., Luchko, T., Gusarov, S., Kovalenko, A. and Kollman P.A. (2010), AMBER 11, University of California, San Francisco.

Chen, D., Lawton, D., Thompson, M.R. and Liu, Q. (2012) Biocomposites reinforced with cellulose nanocrystals derived from potato peel waste. Carbohydrate Polymers, 90, 709-716.

Chhabra, R., Moralez, J.G., Raez, J., Yamazaki, T., Cho, J.-Y., Myles, A.J., Kovalenko, A. and Fenniri, H. (2010) One-Pot Nucleation, Growth, Morphogenesis, and Passivation of 1.4 nm Au Nanoparticles on Self-Assembled Rosette Nanotubes. J. Am. Chem. Soc., 132, 32-33.

Costa, L.M., Hayaki, S., Stoyanov, S.R., Gusarov, S., Tan, X., Gray, M.R., Stryker, J.M., Tykwinski, R., Carneiro, J.W.M., Sato, H., Seidl, P.R. and Kovalenko, A. (2012) 3D-RISM-KH Molecular Theory of Solvation and Density Functional Theory Investigation of the Role of Water in the Aggregation of Model Asphaltenes. Phys. Chem. Chem. Phys., 14, 3922–3934.

Cranston, E.D. and Gray, D.G. (2006) Formation of Cellulose-based Electrostatic Layer-by-layer Films in a Magnetic Feld. Sci. Technol. Adv. Mater., 7, 319-321.

Damm, W., Frontera, A., Tirado-Rives, J. and Jorgensen, W.L. (2001) OPLS All-atom Force Field for Carbohydrates. J. Phys. Chem. B, 105, 6474-6487

de Mesquita, J.P., Donnici, C.L., Teixeira, I.F. and Pereira, F.V. (2012) Bio-based Nanocomposites Obtained through Covalent Linkage Between Chitosan and Cellulose Nanocrystals. Carbohydrate Polymers, 90, 210-217.

Discover (2001) Release 4.0; Accelrys, Inc., CA, USA.

- Dong, X.M., Kimura, T., Revol, J.F. and Gray, D.G. (1996) Effects of Ionic Strength on the Isotropic-Chiral Nematic Phase Transition of Suspensions of Cellulose Crystallites. Langmuir, 12, 2076–2082.
- **Dorris, A. and Gray, D.G.** (2012) Gelation of cellulose nanocrystal suspensions in glycerol. Cellulose, 19, 687-694.
- Ellazzouzi-Hafraouzi, S., Nishiyama, Y., Putaux, J-L., Heux, L., Dubreuil, F. and Rochas, C. (2008) The shape and size distribution of crystalline nanoparticles prepared by acid hydrolysis of native cellulose..Biomacromolecules, 9, 57-65.
- Fafard, J., Lyubimova, O., Stoyanov, S.R., Dedzo, G.K., Gusarov, S., Kovalenko, A. and Detellier, C. (2013) Adsorption of Indole on Kaolinite in Non-aqueous Media: Organoclay Preparation, Characterization, and Investigation by the 3D-RISM-KH Molecular Theory of Solvation. J. Phys. Chem. C. 117 (36), 18556–18566.
- **Freindorf, M. and Gao, J.** (1996) Optimization of the Lennard-Jones Parameters for a Combined Ab Initio Quantum Mechanical and Molecular Mechanical Potential Using the 3-21G Basis Set. J. Comput. Chem., 17, 386-395.
- **Genheden, S., Luchko, T., Gusarov, S., Kovalenko, A. and Ryde, U.** (2010) An MM/3D-RISM Approach for Ligand-Binding Affinities, J. Phys. Chem. B, 114, 8505-8516.
- Gousse, C., Chanzy, H., Excoffier, G., Soubeyrand, L. and Fleury, E. (2002) Stable suspensions of partially silylated cellulose whiskers dispersed in organic solvents. Polymer, 43, 2645-2651.
- **Gusarov, S., Ziegler, T. and Kovalenko, A.** (2006) Self-Consistent Combination of the Three-Dimensional RISM Theory of Molecular Solvation with Analytical Gradients and the Amsterdam Density Functional Package. J. Phys. Chem. A, 110, 6083-6090.
- **Gusarov, S., Pujari, B. S. and Kovalenko, A.** (2012) Efficient treatment of solvation shells in 3D molecular theory of solvation. J. Comput. Chem., 33, 1478-1494.
- **Habibi, Y., Lucia, L.A. and Rojas, O.J.** (2010) Cellulose Nanocrystals: Chemistry, Self-Assembly, and Applications. Chem. Rev., 110, 3479-3500.
- **Hamad, W.** (2006) On the Development and Applications of Cellulosic Nanofibrillar and Nanocrystalline Materials. Can. J. Chem. Eng., 84, 513-519.
- Hanley, S.J., Revol, J-F., Godbout, L. and Gray, D.G. (1997) Atomic Force Microscopy and Transmission Electron Microscopy of Cellulose from Micrasterias Denticulata; Evidence for a Chiral Helical Microfibril Twist. Cellulose, 4, 209-220.
- Hasani, M., Cranston, E.D., Estman, G. and Gray, D.G. (2008) Cationic surface functionalization of cellulose nanocrystals. Soft Matter, 4, 2238-2244.
- Holt, B.L., Stoyanov, S.D., Pelan, E. and Paunov, V.N. (2010) Novel anisotropic materials from functionalised colloidal cellulose and cellulose derivatives. J. Mater. Chem., 20, 10058-10070.
- **Jiang, F., Esker, A.R. and Roman, M.** (2010) Acid-Catalyzed and Solvolytic Desulfation of H2SO4-Hydrolyzed Cellulose Nanocrystals. Langmuir, 26, 17919–17925.
- Johnson, R.S., Yamazaki, T., Kovalenko, A. and Fenniri, H. (2007) Molecular Basis for Water-Promoted Supramolecular

- Chirality Inversion in Helical Rosette Nanotubes. J. Am. Chem. Soc., 129, 5735-5743.
- Kelly, J.A., Shopsowitz, K.E., Ahn, J.M., Hamad, W.Y. and MacLachlan, M.J. (2012) Chiral Nematic Stained Glass: Controlling the Optical Properties of Nanocrystalline Cellulose-Templated Materials. Langmuir, 28, 17256-17262.
- Kelly, J.A., Shukaliak, A.M., Cheung, C.C.Y., Shopsowitz, K.E., Hamad, W.Y. and MacLachlan, M.J. (2013) Responsive Photonic Hydrogels Based on Nanocrystalline Cellulose. Angew. Chem. Int. Ed. Engl., 52, 8912-8916.
- Khan, R.A., Beck, S., Dussault, D., Salmieri, S., Bouchard, J. and Lacroix, M. (2013) Mechanical and Barrier Properties of Nanocrystalline Cellulose Reinforced Poly(caprolactone) Composites: Effect of Gamma Radiation. J. Appl. Polymer Sci. 2013, 129, 3038-3046.
- Kirschner, K.N., Yongye, A.B., Tschampel, S.M., González-Outeiriño, J., Daniels, C.R., Foley, B.L. and Woods, R.J. (2008) GLYCAM06: A generalizable biomolecular force field. Carbohydrates. *J. Comput. Chem.*, 29, 622-655.
- **Kobryn, A.E. and Kovalenko, A.** (2008) Molecular Theory of Hydrodynamic Boundary Conditions in Nanofluidics. J. Chem. Phys., 129, 134701-134716.
- Kobryn, A., Nikolic, D., Lyubimova, O., Gusarov, A. and Kovalenko, A. (2014) DPD with an Effective Pair Potential Obtained from Integral Equation Theory of Molecular Liquids, Soft Matter, (submitted).
- Koneshan, S., Jayendran, C.R., Lynden-Bell, R.M. and Lee, S.H. (1998) Solvent Structure, Dynamics, and Ion Mobility in Aqueous Solutions at 25°C. J. Phys. Chem. B, 102, 4193–4204.
- **Kovalenko, A.** (2003) Three-dimensional RISM Theory for Molecular Liquids and Solid-liquid Interfaces, in Understanding Chemical Reactivity: Molecular Theory of Solvation, F. Hirata, ed., Kluwer Academic Publishers, 24, pp.169-275.
- **Kovalenko, A.** (2004) Molecular Description of Electrosorption in a Nanoporous Carbon Electrode. J. Comput. Theor. Nanosci., 1, 398-411.
- **Kovalenko, A.** (2013) Multiscale Modeling of Solvation in Chemical and Biological Nanosystems and in Nanoporous Materials. Pure Appl. Chem., 85, 159-199.
- **Kovalenko, A. and Hirata, F.** (1999) Self-Consistent Description of a Metal–Water Interface by the Kohn–Sham Density Functional Theory and the Three-Dimensional Reference Interaction Site. J. Chem. Phys., 110, 10095-10112.
- **Kovalenko, A., Ten-no, S. and Hirata, F.** (1999) Solution of the three-dimensional RISM/HNC equations for SPC water by the modified method of direct inversion in the iterative subspace. J. Comput. Chem., 20, 928-936.
- **Kovalenko, A. and Hirata, F.** (2000a) Potentials of Mean Force of Simple lons in Ambient Aqueous Solution. I: Three-dimensional Reference Interaction Site Model Approach. J. Chem. Phys., 112, 10391-10402.
- **Kovalenko, A. and Hirata, F.** (2000b) Potentials of mean force of simple ions in ambient aqueous solution. II. Solvation structure from the three-dimensional reference interaction site model approach, and comparison with simulations. J. Chem. Phys., 112, 10403-10417.

- **Kovalenko A. and Hirata, F.** (2001a) First-principles Realization of a van der Waals-Maxwell Theory for Water. Chem. Phys. Lett., 349, 496-502.
- **Kovalenko, A. and Hirata, F.** (2001b) A Replica Reference Interaction Site Model Theory for a Polar Molecular Liquid Sorbed in a Disordered Microporous Material with Polar Chemical Groups. J. Chem. Phys., 115, 8620-8633.
- **Kovalenko A. and Hirata, F.** (2002) Towards a Molecular Theory for the Van Der Waals–Maxwell Description of Fluid Phase Transitions. J. Theor. Comput. Chem., 1, 381-406.
- Kovalenko, A., Kobryn, A.E., Gusarov, S., Lyubimova, O., Liu, X., Blinov N. and Yoshida, M. (2012) Molecular Theory of Solvation for Supramolecules and Soft Matter Structures: Application to Ligand Binding, Ion Channels, and Oligomeric Polyelectrolyte Gelators. Soft Matter, 8, 1508-1520.
- Lacmann, R. and Synowietz C. (1974) Densities of Liquid Systems. Part A: Nonaqueous Systems and Ternary Aqueous Systems, Landolt-Börnstein New Series, Group IV, Vol. 1, Schäfer, K.I., ed. Springer-Verlag, Berlin, Germany.
- Lahiji, R.R., Xu, X., Reifenberger, R., Raman, A., Rudie, A. and Moon, R.J. (2010) Atomic Force Microscopy Characterization of Cellulose Nanocrystals. Langmuir, 26, 4480-4488, and references therein.
- Li, Q., Gusarov, S., Evoy, S. and Kovalenko, A. (2009) Electronic Structure, Binding Energy, and Solvation Structure of the Streptavidin-Biotin Supramolecular Complex: ONIOM and 3D-RISM Study. J. Phys. Chem. C, 113, 9958-9967.
- **Lin, N. and Dufresne, A.** (2013) Supramolecular Hydrogels from In Situ Host-guest Inclusion Between Chemically Modified Cellulose Nanocrystals and Cyclodextrin. Biomacromolecules, 14, 871-880.
- **Liu, X., Lyubimova, O., Kobryn, A.E., Gusarov S. and Kovalenko, A.** (2011) Mesoscopic Study of Dynamics and Gelation Ability of Oligomeric Electrolyte Gelator with Dissipative Particle Dynamics. Proc. Comput. Sci., 4, 1031-1038.
- **Lynden-Bell, R.M., Atamas, N.A., Vasilyuk., A. and Hanke, C.G.** (2002) Chemical Potentials of Water and Organic Solutes in Imidazolium Ionic Liquids: A Simulation Study. Mol. Phys., 100, 3225-3229.
- Lyubimova, O., Liu, X., Gusarov, S., Kobryn A.E. and Kovalenko, A. (2011) Solvation Structure and Gelation Ability of Polyelectrolytes: Predictions by Quantum Chemistry Methods and Integral Equation Theory of Molecular Liquids. Proc. Comput. Sci., 4, 1186-1192.
- Lyubimova, O., Stoyanov, S.R., Gusarov, S., and Kovalenko, A. (2014) Solvation Effects and Structure Relaxation of Modified Cellulose Nanocrystals in Aqueous Electrolyte Solution: Predictions by Molecular Dynamics and Molecular Theory of Solvation. Biomacromolecules, (submitted).
- Malvaldi, M., Bruzzone, S., Chiappe, C., Gusarov, S. and Kovalenko, A. (2009) Ab Initio Study of Ionic Liquids by KS-DFT/3D-RISM-KH Theory. J. Phys. Chem. B, 113, 3536-3542.
- Maple, J.R., Dinur, U. and Hagler, A.T. (1988) Derivation of Force Fields for Molecular Mechanics and Dynamics from Ab Initio Energy Surfaces. Proc. Natl. Acad. Sci. 85, 5350-5354.
- Matthews, J.F., Bergenstrahle, M., Beckham G.T., Himmel, M.E., Nimlos, M.R., Brady, J.W. and Crowley, M.F.J. (2011)

- High-Temperature Behavior of Cellulose I. J. Phys. Chem. B, 115, 2155-2166.
- Matthews, J.F., Skopec, C.E., Mason, P.E., Zuccato, P., Torget, R.W., Sugiyama, J., Himmel, M.E. and Brady. J.W. (2006) Computer Simulation Studies of Microcrystalline Cellulose Iβ. Carbohydrate Research, 341, 138-152.
- **Matubayashi, N. and Nakahara, M.** (2000) Theory of Solutions in the Energetic Representation. I. Formulation. J. Chem. Phys. 113, 6070–6081.
- Montanari, S., Roumani, M., Heux, L. and Vignon, M.R. (2005) Topochemistry of Carboxylated Cellulose Nanocrystals Resulting from TEMPO-Mediated Oxidation. Macromolecules, 38, 1665-1671.
- Moralez, J.G., Raez, J., Yamazaki, T., Motkuri, R.K., Kovalenko, A. and Fenniri, H. (2005) Helical Rosette Nanotubes with Tunable Stability and Hierarchy. J. Am. Chem. Soc. 127, 8307-8309.
- Nikolic, D., Moffat, K.A., Farrugia, V.M., Kobryn, A.E., Gusarov, S., Wosnick, J.H. and Kovalenko, A. (2013) Multiscale Modeling and Synthesis of Polyester Ionomers. Phys. Chem. Chem. Phys., 15, 6128-6138.
- Nishiyama, Y., Langan, P. and Chanzy, H. (2002) Crystal Structure and Hydrogen-Bonding System in Cellulose I β from Synchrotron X-ray and Neutron Fiber Diffraction. J. Am. Chem. Soc., 124, 9074-9082.
- **Nishiyama, Y., Sugiyama, J., Chanzy, H. and Langan, P.** (2003) Crystal Structure and Hydrogen Bonding System in Cellulose Iα from Synchrotron X-ray and Neutron Fiber Diffraction. J. Am. Chem. Soc., 125, 14300-14306.
- **Paavilainen, S., Rog, T. and Vattulainen, I.J.** (2011) Analysis of Twisting of Cellulose Nanofibrils in Atomistic Molecular Dynamics Simulations. Phys. Chem. B, 115, 3747-3755.
- **Perkyns, J.S. and Pettitt, B.M.A.** (1992a) Site-site Theory for Finite Concentration Saline Solutions. J. Chem. Phys., 97, 7656-7666.
- **Perkyns, J.S. and Pettitt, B.M.A.** (1992b) Dielectrically Consistent Interaction Site Theory for Solvent-electrolyte Mixtures. Chem. Phys. Lett., 190, 626-630.
- Picard, G., Simon, D., Kadiri, Y., LeBreux, J.D. and Ghozayel, F. (2012) Cellulose Nanocrystal Iridescence: A New Model. Langmuir, 28, 14799-14807.
- Postek, M.T., Vladar, A., Dagata, J., Farkas, N. and Ming, B. (2008) Cellulose Nanocrystals the Next Big Nano-thing? Proc. SPIE, 7042, 70420D.
- **Qian, X.** (2008) The Effect of Cooperativity on Hydrogen Bonding Interactions in Native Cellulose I β from Ab Initio Molecular Dynamics Simulations. Molec. Simul., 34, 183-191.
- **Shen, T. and Gnanakaran, S.** (2009) The Stability of Cellulose: A Statistical Perspective from a Coarse-Grained Model of Hydrogen-Bond Networks. Biophys. J., 96, 3032-3040.
- Shen, T., Langan, P., French, A.D., Johnson, G.P. and Gnanakaran, S. (2009) Conformational Flexibility of Soluble Cellulose Oligomers: Chain Length and Temperature Dependence. J. Am. Chem. Soc., 131, 14786-14794.
- **Shopsowitz, K.E., Hamad, W.Y. and MacLachlan, M.J.** (2012) Flexible and Iridescent Chiral Nematic Mesoporous Organosilica Films. J. Am. Chem. Soc., 134, 867-870.

- Silveira, R. L.; Stoyanov, S. R.; Gusarov, S.; Skaf, M. S. and Kovalenko, A. (2013) Plant Biomass Recalcitrance: Effect of Hemicellulose Composition on Nanoscale Forces that Control Cell Wall Strength. J. Am. Chem. Soc. 135, 19048–19051.
- **Siqueira, G., Bras, J., and Dufresne, A.** (2010) Cellulosic Bionanocomposites: A Review of Preparation, Properties and Applications. Polymers, 2, 728-765.
- **Stoyanov, S.R., Gusarov, S. and Kovalenko, A.** (2008) Multiscale Modeling of Asphaltene Disaggregation. Mol. Simul., 34, 953-960.
- **Stoyanov, S.R., Gusarov, S. and Kovalenko, A.** (2011) Multiscale Modeling of the Adsorption Interaction Between Model Bitumen Compounds and Zeolite Nanoparticles in Gas and Liquid Phase, In Industrial Applications of Molecular Simulations, Meunier, M., Ed.; Taylor and Francis Books: Boca Raton, FL, USA, pp. 203-230.
- Stoyanov, S.R., Gusarov, S. and Kovalenko, A. (2013) Multiscale Modeling of Solvation and Effective Interactions of Functionalized Cellulose Nanocrystals. In Production and Applications of Cellulose Nanomaterials. Postek, M. T.; Moon, R. J.; Rudie, A.; Bilodeau, M., Eds.; TAPPI Press, Atlanta, GA, USA, pp. 147–150.
- Stumpe, M.C., Blinov, N., Wishart, D., Kovalenko, A. and Pande, V.S. (2011) Calculation of Local Water Densities in Biological Systems: A Comparison of Molecular Dynamics Simulations and the 3D-RISM-KH Molecular Theory of Solvation. J. Phys. Chem. B, 115, 319-328.
- Sun, H., Mumby, S.J., Maple, J.R. and Hagler, A.T. (1994) An ab Initio CFF93 All-Atom Force Field for Polycarbonates. J. Amer. Chem. Soc., 116, 2978-2987.
- **Swart, M., van Duijnen, P.T. and Snijders, J.P.** (2001) A Charge Analysis Derived from an Atomic Multipole Expansion. J. Comput. Chem., 22, 79-88.
- **Tanimura, A., Kovalenko, A. and Hirata, F.** (2007) Structure of Electrolyte Solutions Sorbed in Carbon Nanospaces, Studied by the Replica RISM Theory. Langmuir, 23, 1507-1517.
- Wang, N., Ding, E. and Cheng, R. (2007) Surface modification of cellulose nanocrystals. Front. Chem. Eng China, 1, 228.
- **Welton, T. and Wasserschield, P.** (2007) Ionic Liquids in Synthesis. VCH-Wiley, Weinheim,.
- Wik, V.M., Aranguren, M.I. and Mosiewicki, M.A. (2011) Castor Oil-based Polyurethanes Containing Cellulose Nanocrystals. Polymer Eng. & Sci., 51, 1389-1396.
- Wohlfarth, C. (1991) Static Dielectric Constants of Pure Liquids and Binary Liquid Mixtures, Landolt-Börnstein New Series, Group IV, Vol. 6, Madelung, O., ed. Springer-Verlag, Berlin, Germany.
- Yamazaki, T., Blinov, N., Wishart, D. and Kovalenko, A. (2008) Hydration Effects on the HET-s Prion and Amyloid-β Fibrillous Aggregates, Studied with 3D Molecular Theory of Solvation. Biophys. J., 95, 4540-4548.
- Yamazaki, T., Fenniri, H. and Kovalenko, A. (2010) Structural Water Drives Self-assembly of Organic Rosette Nanotubes and Holds Host Atoms in the Channel. ChemPhysChem, 11, 361-367.
- **Yamazaki, T. and Kovalenko, A.** (2009) Spatial Decomposition Analysis of the Thermodynamics of Cyclodextrin Complexation. J. Chem. Theory Comput., 5, 1723–1730.

- Yang, J., Han, C.-R., Duan, J.-F., Xu, F. and Sun, R.-C. (2013) Mechanical and Viscoelastic Properties of Cellulose Nanocrystals Reinforced Poly(ethylene glycol) Nanocomposite Hydrogels. ACS Appl. Mater. Interfaces, 5, 3199-3207.
- Yoshida, K., Yamaguchi, T., Kovalenko, A. and Hirata, F. (2002) Hydration Effects on the HET-s Prion and Amyloid- β Fibrillous Aggregates, Studied with Three-Dimensional Molecular Theory of Solvation. J. Phys. Chem. B, 106, 5042-5049.
- Yui, T. and Hayashi, S. (2007) Molecular Dynamics Simulations of Solvated Crystal Models of Cellulose I α and III_I. Biomacromolecules, 8, 817-824.
- Yui, T., Shiiba, H., Tsutsumi, H., Hayashi, S., Miyata, T. and Hirata, F. (2010) Systematic Docking Study of the Carbohydrate Binding Module Protein of Cel7A with the Cellulose Iα Crystal Model. J. Phys. Chem. B, 114, 49.
- Zainuddin, S.Y.Z., Ahmad, I., Kargarzadeh, H., Abdullah, I. and Dufresne, A. (2013) Potential of Using Multiscale Kenaf Fibers as Reinforcing Filler in Cassava Starch-kenaf Biocomposites. Carbohydrate Polymers, 92, 2299-2305.
- **Zhang, Y.P., Chodavarapu, V.P., Kirk, A.G. and Andrews, M.P.** (2012) Nanocrystalline Cellulose for Covert Optical Encryption. J. Nanophoton., 6, 063516.

Manuscript received November 15, 2013 Accepted February 18, 2014